

# Catalysis Science & Technology

Accepted Manuscript



This article can be cited before page numbers have been issued, to do this please use: X. Zhang, X. Cheng, M. Chuanyuan and Z. Wang, *Catal. Sci. Technol.*, 2018, DOI: 10.1039/C8CY00709H.



This is an Accepted Manuscript, which has been through the Royal Society of Chemistry peer review process and has been accepted for publication.

Accepted Manuscripts are published online shortly after acceptance, before technical editing, formatting and proof reading. Using this free service, authors can make their results available to the community, in citable form, before we publish the edited article. We will replace this Accepted Manuscript with the edited and formatted Advance Article as soon as it is available.

You can find more information about Accepted Manuscripts in the [author guidelines](#).

Please note that technical editing may introduce minor changes to the text and/or graphics, which may alter content. The journal's standard [Terms & Conditions](#) and the ethical guidelines, outlined in our [author and reviewer resource centre](#), still apply. In no event shall the Royal Society of Chemistry be held responsible for any errors or omissions in this Accepted Manuscript or any consequences arising from the use of any information it contains.



## Effects of Fe/Ce ratio on the catalytic activity of CuO/CeO<sub>2</sub>-Fe<sub>2</sub>O<sub>3</sub> catalysts for NO reduction by CO

Xingyu Zhang<sup>ab</sup>, Xingxing Cheng<sup>\*ab</sup>, Chunyuan Ma<sup>\*ab</sup> and Zhiqiang Wang<sup>ab</sup>

Received 00th April 20xx,  
Accepted 00th April 20xx

DOI: 10.1039/x0xx00000x

[www.rsc.org/](http://www.rsc.org/)

Copper catalysts on Fe-loaded ceria were studied for NO reduction by CO. The catalyst with different Fe/Ce molar ratio (Cu/C<sub>1</sub>F<sub>x</sub>) were synthesized by impregnation method. The catalysts were characterized by XRD, BET, Raman, EPR, H<sub>2</sub>-TPR and in situ DRIFT spectra. CuO was highly dispersed on support surface to form active species. The ceria modification by incorporation of lower Fe<sup>3+</sup> amount is beneficial for NO conversion and the N<sub>2</sub> selectivity as compared with the pure ceria and iron-rich ones, which would be resulted from the strong interaction between ceria and iron. Cu/C<sub>1</sub>F<sub>1</sub> showed better catalytic performance at 100-200 °C, while Cu/C<sub>1</sub>F<sub>0.5</sub> gave the higher N<sub>2</sub> selectivity than other samples. In situ DRIFT results suggested that rich-iron catalysts ensured an inhibition of the reduction of NO by increased NO partial pressures. There exists two mechanisms that form the NCO intermediate and N<sub>2</sub>O intermediate over ceria-rich catalysts. With the increasing of Fe/Ce molar ratio and temperature, The mechanism of N<sub>2</sub>O as intermediate dominate the reaction, while the process that produced NCO species as intermediate gradually disappear.

### A Headings are the primary heading type e.g. Introduction, Results and discussion, Experimental

The abatement of NO<sub>x</sub> from the combustion of fossil fuel is of great importance for environmental protection.<sup>1-6</sup> Nitric oxide reduction by CO is a new technology in the removal of NO<sub>x</sub> from stationary sources emission using rotary reactor.<sup>7-9</sup> The catalyst with excellent performance not only could be used at the reactor work as the medium of NO<sub>x</sub> adsorbed and reduced, but also could reduced the desorption NO<sub>x</sub> from the surface of the catalyst by CO in the reducing gas. Meanwhile, low reaction temperatures are of great significance for cost savings. Hence, the catalyst with superior catalytic activity at low temperature exhibit multifunctional application potential.

For NO + CO reaction, many efforts have been spent on

investigating the performance over various supported noble metal catalysts, such as Pd/Al<sub>2</sub>O<sub>3</sub>,<sup>10</sup> Rh/Al<sub>2</sub>O<sub>3</sub>,<sup>11</sup> Pt/WO<sub>3</sub>/CeO<sub>2</sub>/ZrO<sub>2</sub>,<sup>12</sup> Pt/SBA-15,<sup>13</sup> Au/CeO<sub>2</sub>-M<sub>2</sub>O<sub>3</sub> (M = Al, La),<sup>14</sup> Ir/WO<sub>3</sub>-SiO<sub>2</sub>.<sup>15</sup> In recent years, ceria (CeO<sub>2</sub>) has been received increasing attentions and found tremendous applications in environmental catalysis due to its high oxygen storage-release capacity associated with Ce<sup>4+</sup>/Ce<sup>3+</sup> redox cycle.<sup>16, 17</sup> When doped with Cu<sup>+</sup> ions, ceria acts as highly active deNO<sub>x</sub> catalysts with high resistance to H<sub>2</sub>O and SO<sub>2</sub> poisoning.<sup>18</sup> Nevertheless, it still showed the unsatisfactory activity and selectivity for NO reduction at low temperature, especially for the stability of the catalysts structure. Generally, the most studied component of the catalysts has been cerium oxide since it is able to stabilizes the dispersion of active metal oxides and it stores and releases oxygen.<sup>19</sup> Therefore, many studies worldwide aim at improve efficiency and stability by introducing other promoters, such as alumina,<sup>1, 20</sup> zinc,<sup>21</sup> stannum,<sup>22</sup> cobalt,<sup>23</sup> molybdenum,<sup>24, 25</sup> magnesium,<sup>26</sup> and zirconia.<sup>27-30</sup>

The nature of dopant plays an important role for ceria modification, and the interaction between ceria and dopant could promote the catalysis. Research shows that doped-ceria with trivalent ions (Pr<sup>3+</sup> and Tb<sup>3+</sup>) result in a lowering of the energy

<sup>a</sup> National Engineering Lab for Coal-fired Pollutants Emission Reduction, Shandong University, Jinan 250061, PR China. email: chym@sdu.edu.cn, xcheng@sdu.edu.cn

<sup>b</sup> Provincial Key Lab of Energy Carbon Reduction and Resource Utilization, Shandong University, Jinan 250061, PR China

Electronic Supplementary Information (ESI) available: [details of any supplementary information available should be included here]. See DOI: 10.1039/x0xx00000x

## ARTICLE

## Journal Name

barrier for oxygen migration,<sup>31,32</sup> this seems to be beneficial for the formation of oxygen vacancies. Whereas the outstanding performance of Fe<sub>2</sub>O<sub>3</sub> for redox capacity and N<sub>2</sub>O reduction by CO draw our attention.<sup>33</sup> Hence, it was expected that combining the advantages of CuO/CeO<sub>2</sub> system and iron oxides promoter to achieve the goal of high reactivity and low cost.

In this paper, we systematically synthesized a series of Cu/CeO<sub>2</sub>-Fe<sub>2</sub>O<sub>3</sub> composites with the Fe atomic ratio (Ce balance) varying from 0 to 100%. Their structures were characterized by means of X-ray diffraction (XRD), BET surface area measurement, Raman spectroscopy, and Electron Paramagnetic Resonance (EPR). The catalytic performance of Cu/CeO<sub>2</sub>-Fe<sub>2</sub>O<sub>3</sub> composites in NO reduction by CO was also tested. The role of Fe on Cu/CeO<sub>2</sub>-Fe<sub>2</sub>O<sub>3</sub> is discussed. The purpose of the present work is not only to assess the deNO<sub>x</sub> capability of the Cu/CeO<sub>2</sub>-Fe<sub>2</sub>O<sub>3</sub> catalysts, but more importantly to clarify the nature of Fe-doped for catalytic performance.

## 2. Experiments

### Catalysts preparation

The mixed oxides of CeO<sub>2</sub> and Fe<sub>2</sub>O<sub>3</sub> are prepared by co-precipitation method. The requisite amount of Ce(NO<sub>3</sub>)<sub>3</sub>·6H<sub>2</sub>O as Ce source and Fe(NO<sub>3</sub>)<sub>3</sub>·9H<sub>2</sub>O as Fe source was dissolved into distilled water to form solution. After being stirred for 1h, the solution was evaporated in air at 160 °C for 2h, and then calcinated in air at 550 °C for 3h. The as-prepared CeO<sub>2</sub>-Fe<sub>2</sub>O<sub>3</sub> oxide supports were hereafter denoted as CF. In addition, pure CeO<sub>2</sub> and Fe<sub>2</sub>O<sub>3</sub> were prepared via the same procedure for comparison. The Cu/CF catalysts were prepared by wetness impregnation method with Cu(NO<sub>3</sub>)<sub>2</sub> solution. The mixture was kept in stirring 1h, dried in air at 160 °C for 2h, and finally calcinated in air at 550 °C for 3h. Catalysts with individual oxide CeO<sub>2</sub> and Fe<sub>2</sub>O<sub>3</sub> support are named as Cu/Ce and Cu/Fe, respectively. Some main properties of the prepared catalysts are summarized in Table 1.

### Catalyst characterization

The specific surface area was investigated by nitrogen adsorption at 77 K (Quantachrome Autosorb-iQ) using the BET method. The pore volume and average pore diameter were derived from the BJH method. XRD patterns were recorded on a Philips X'Pert Pro diffractometer, equipped with a Ni-filtered Cu K radiation (0.15418 nm). The X-ray tube was operated at 40 kV and 40 mA. The data were collected in the 2θ range of 10–80°. The average crystallite sizes

(D<sub>XRD</sub>) were determined from XRD line broadening measurements using the Scherrer equation,  $D_{XRD} = \frac{\lambda}{\beta \cos \theta}$ , where λ is the X-ray wavelength, θ is the diffraction angle, K is the particle shape factor, usually taken as 0.89, and β is full width at half maximum in radians. Raman spectra were collected on a Jobin-Yvon (France-Japan) T64000 type Raman spectroscopy using Ar<sup>+</sup> laser beam. The Raman spectra were recorded with an excitation wavelength at 514nm and the laser power at 300mW. The EPR spectra were recorded on a EPR spectrometer (JEOL-FE-1X) operating in the X-band frequency (≈9.200 GHz) with a field modulation frequency of 100 kHz. The magnetic field was scanned from 0 to 500mT and the microwave power used was 5mW. The measurements were made at room temperature. H<sub>2</sub>-TPR experiments were performed in a quartz U-type reactor, and 50 mg sample was used for each measurement. Prior to the reduction, the catalyst was pretreated in N<sub>2</sub> stream at 120 °C for 1 h and then cooled to room temperature. After that, H<sub>2</sub>-Ar mixture (10% H<sub>2</sub> by volume) was switched on, and the temperature increased gradually with a ramp of 10 °C/min. The H<sub>2</sub> consumption was monitored using a thermal conduction detector (TCD). In situ DRIFTS spectra was collected at 300°C temperature on a Nicolet 6700 FT-IR spectrometer, working in the range of wave numbers 650–4000cm<sup>-1</sup> at a resolution of 4 cm<sup>-1</sup> (number of scans, 64). The spectra of empty FTIR cell was collected in NO and CO atmosphere at various target temperatures as background. The catalysts (~10 mg) were mounted in a quartz FTIR cell and pretreated for 1 h at 100 °C in flowing Ar atmosphere. After cooled to room temperature, the sample wafers were exposed to a controlled stream of CO-Ar (0.5 % of CO by volume) and NO-Ar mixture (0.2% of NO by volume) at a rate of 50 ml/min for 30 min. Then, the cell was heated at a rate of 10 °C min<sup>-1</sup>. All of the presented spectra were obtained by subtraction of the corresponding background reference.

### Catalytic activity measurement

The catalytic activity experiments were performed in a fixed bed, down flow, quartz reactor (length, 30 cm; inner diameter, 4 mm). The NO + CO reaction was investigated under steady state, involving a fixed feed with a gas composition of 800 ppm NO, 1600 ppm CO and N<sub>2</sub> by volume as a carrier gas at a space velocity of 30,000 h<sup>-1</sup>. For each measurement, 50mg catalyst was pretreated in N<sub>2</sub> stream at 100 °C for 1 h and then be cooled to room temperature. After that, the valve gear was switched to the reaction gas. Concentration of NO, N<sub>2</sub>O, CO and CO<sub>2</sub> at the inlet and

the outlet of the reactor were simultaneously monitored by an online combustion gas analyzer (Gasetm DX-4000, Finland).

### 3. Results and discussion

#### Characterization of catalysts

**Fig. 1** presented the XRD patterns of Cu/CF catalysts. It can be seen that CuO, CeO<sub>2</sub> and  $\alpha$ -Fe<sub>2</sub>O<sub>3</sub> characteristic peaks appear for all the present catalysts. The extremely small CuO peak at about 38.79° indicating that copper oxide was well dispersed in all the catalysts. With the decreasing Ce/Fe ratio, the peak corresponding to cubic fluorite structure of ceria gradually weakened, indicating that the loading of iron reduced the content and crystallinity of ceria. However, no observable shift in diffraction lines of CuO, CeO<sub>2</sub> and  $\alpha$ -Fe<sub>2</sub>O<sub>3</sub> can be found in all catalysts, indicating that there is no change of crystallite structure. From **Table 1**, it could be seen that the crystallite size of  $\alpha$ -Fe<sub>2</sub>O<sub>3</sub> in catalysts increased crystallite size of CeO<sub>2</sub> in catalysts is similar. However, the crystallite size of CuO vary greatly in size and Cu/C<sub>1</sub>F<sub>1</sub> has the smallest crystallite size. Additionally, the decreased of Ce/Fe molar ratio also leads to decreased surface area and pore volume.

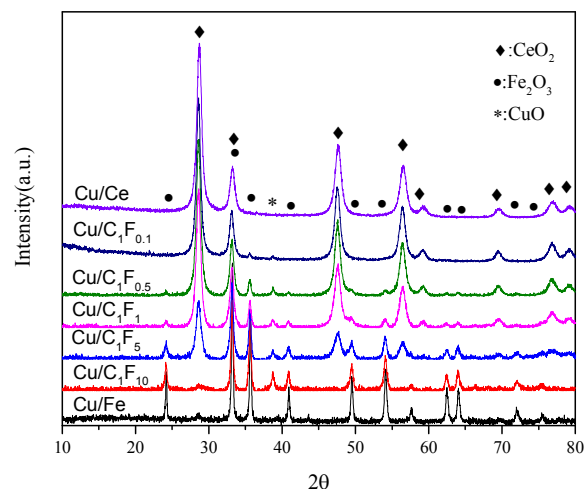


**Fig. 1** XRD patterns of the studied copper catalysts on Fe-doped ceria supports

Raman spectroscopy, as a potential tool and sensitive to metal-oxygen arrangement and lattice defects, was performed to obtain additional structural information<sup>34, 35</sup>. As shown in **Fig. 2**, three typical bands of crystalline CuO at 298, 340, and 628 cm<sup>-1</sup> were not observed, which suggests that copper interaction of Cu and Ce species probably occurred through the formation of a Cu-O-Ce bond. Similar results were also reported by Li et al.<sup>36</sup> Additionally, the strong peak at 458 cm<sup>-1</sup> for the Cu/Ce sample was attributed to triply degenerate F<sub>2g</sub> mode of the fluorite-type lattice, which can be viewed as a symmetric breathing mode of oxygen atoms around cerium ions<sup>37</sup>. The Raman band position and width could be influenced by phonon confinement, strain, defects, and variation in the particle size<sup>38</sup>. Once iron species is introduced, this peak shifts from 458 cm<sup>-1</sup> for the Cu/Ce sample to 451cm<sup>-1</sup> for the Cu/C<sub>1</sub>F<sub>5</sub> sample, and becomes weaker. This shift may imply that slight changes in the lattice parameter with particle size and the

**Table 1** Copper oxide, cerium oxide and iron oxide loading and BET surface area and crystallite size of catalysts

Catalysts	CuO loading (%)	CuO loading (mmol/100m <sup>2</sup> )	Ce/Fe molar ratio	BET surface area(m <sup>2</sup> /g)	Pore Volume (cm <sup>3</sup> /g)	Crystallite size (nm) <sup>a</sup>		
						CuO	Fe <sub>2</sub> O <sub>3</sub>	CeO <sub>2</sub>
Cu/Fe	0.4	0.05	-	10	0.08	22	22	n.d. <sup>b</sup>
Cu/C <sub>1</sub> F <sub>10</sub>	0.4	0.04	1:10	12	0.09	23	25	n.d. <sup>b</sup>
Cu/C <sub>1</sub> F <sub>5</sub>	0.4	0.02	1:5	24	0.11	26	19	12
Cu/C <sub>1</sub> F <sub>1</sub>	0.4	0.013	1:1	38	0.14	20	15	16
Cu/C <sub>1</sub> F <sub>0.5</sub>	0.4	0.01	1:0.5	51	0.15	26	14	13
Cu/C <sub>1</sub> F <sub>0.1</sub>	0.4	0.008	1:0.1	59	0.18	33	13	14
Cu/Ce	0.4	0.0079	-	63	0.22	25	n.d. <sup>b</sup>	12

The crystallite size of CuO, Fe<sub>2</sub>O<sub>3</sub> and CeO<sub>2</sub> from the crystal plane diffraction peak (111), (111) and (104), respectively.

<sup>a</sup> Crystallite size determined from the xrd diffraction peak by Scherrer equation

<sup>b</sup> Not detected

## ARTICLE

## Journal Name

presence of oxygen vacancies<sup>39, 40</sup>, which is related to structural defects derived from interaction of iron and CeO<sub>2</sub>. The appearance of other bands at 284, 400 and 591 cm<sup>-1</sup> for Cu/C<sub>1</sub>F<sub>0.5</sub> attributed to hematite ( $\alpha$ -Fe<sub>2</sub>O<sub>3</sub>) and these peaks shifts from the above to 291, 407 and 606 cm<sup>-1</sup> for Cu/Fe<sup>37, 41, 42</sup>. Meanwhile, the appearance of new bands at 224 and 496 cm<sup>-1</sup> for Cu/C<sub>1</sub>F<sub>1</sub>, Cu/C<sub>1</sub>F<sub>5</sub>, Cu/C<sub>1</sub>F<sub>10</sub> and Cu/Fe attributed to hematite ( $\alpha$ -Fe<sub>2</sub>O<sub>3</sub>) and that was not seen in the other catalysts. Thus, the present results indicate that the presence of over-proportional ceria influences the crystal lattice of iron oxide. Fe<sup>3+</sup> is much easier to occupy the substituted Ce<sup>4+</sup> sites in the CeO<sub>2</sub> lattice as the concentration of doped Fe<sup>3+</sup> is below the critical value and prefers to become interstitial within the ceria structure when the concentration of doped Fe<sup>3+</sup> surpasses the critical value<sup>37</sup>. As it was reported that a change of the particle size of CeO<sub>2</sub> from 6 nm to 5  $\mu$ m led to a shift in peak position about 10 cm<sup>-139, 40</sup>. However, in the case of the XRD results, all catalysts have similar crystallite size of CeO<sub>2</sub>, the results of Raman and XRD characteristic peaks of these Cu/C<sub>1</sub>F<sub>x</sub> catalysts suggest may only lower Fe<sup>3+</sup> amount could incorporate into ceria oxide lattice and the vast majority of Fe still exist in the form of Fe<sub>2</sub>O<sub>3</sub>.

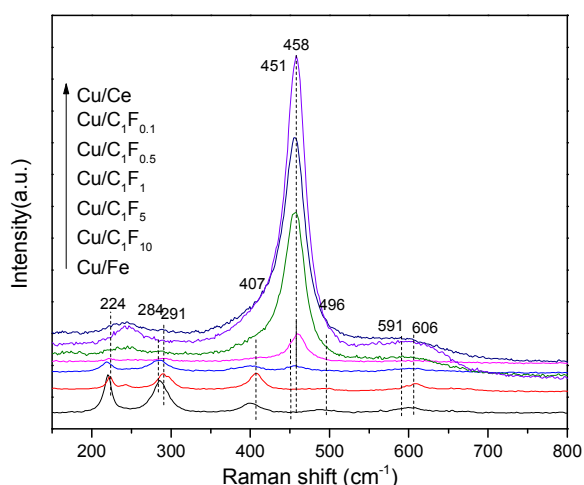
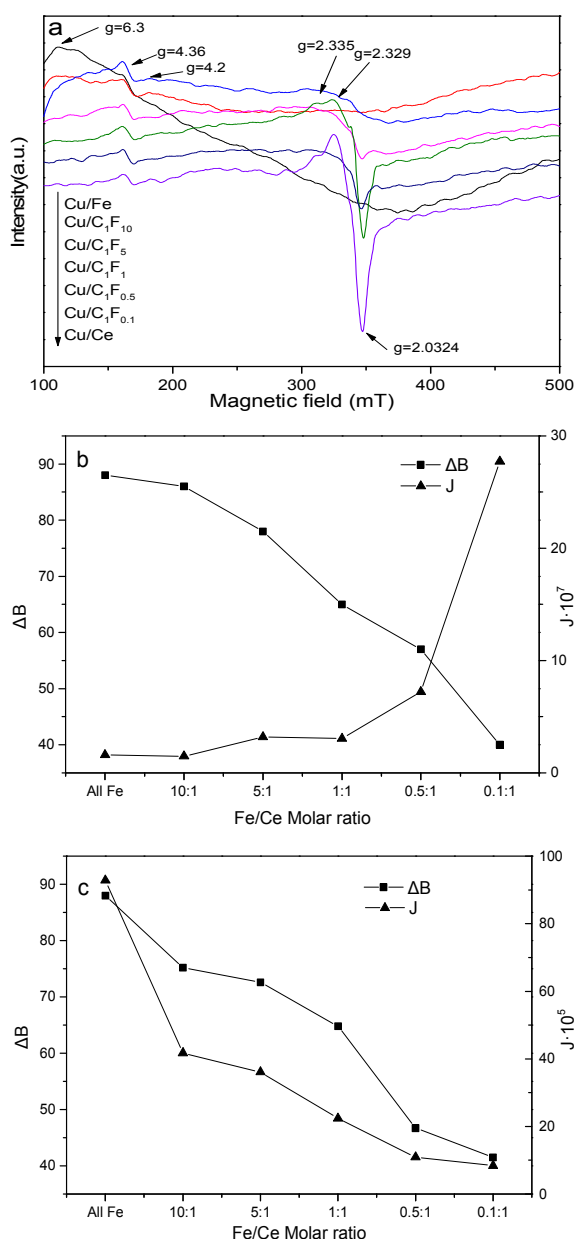


Fig. 2 Raman spectra of the studied copper catalysts on iron-ceria supports

EPR was performed to investigate the surface oxidation states, the physical form of the transition metal oxides, and some synergetic interactions on the surface. Fig. 3a shows the spectra of the representative catalysts. The EPR spectra exhibit multiple signals of copper, the signal that showing unresolved parallel component at  $g=2.040$ , is ascribed to the copper(II) ion pairs in ceria, i.e., the substitution of two Cu<sup>2+</sup> ions for two neighboring Ce<sup>4+</sup>

ions in the lattice with the smallest distance (3.811 Å). This substitution only occurs on the surface and does not destroy the matrix structure of Fe<sub>2</sub>O<sub>3</sub> and CeO<sub>2</sub>. Compared with Cu/Fe, Cu/Ce shows stronger signal, indicating that the larger specific surface area of CeO<sub>2</sub> promotes the dispersion of Cu<sup>2+</sup> and the substitution of Cu<sup>2+</sup> for Ce<sup>4+</sup>. However, when both of Fe<sub>2</sub>O<sub>3</sub> and CeO<sub>2</sub> are introduced, the signal intensity decreases with Fe/Ce molar ratio. The reason is easy to understand that the doping of undispersible Cu<sup>2+</sup> is difficult when specific surface area of Cu/C<sub>1</sub>F<sub>x</sub> decreases. The signals at  $g = 2.329$  and  $g = 2.335$ , are contributed by isolated Cu<sup>2+</sup> in octahedral sites of ceria with a tetragonal distortion and in surface substitution sites of ceria, respectively<sup>43</sup>. Meanwhile, a typical EPR spectrum for Fe<sup>3+</sup> ions in Cu/Fe, Cu/C<sub>1</sub>F<sub>10</sub> and Cu/C<sub>1</sub>F<sub>1</sub> catalysts. The EPR spectra mainly consists of an intense resonance signal at  $g=4.3$ , it can be attributed to the isolated free Fe<sup>3+</sup> (smaller iron oxides phases). In particular for Cu/Fe, the EPR spectrum shows a shoulder in the region of  $g\approx 6.3$ . The  $g$  value of Fe<sup>3+</sup> is expected to lie very near the free-ion value and the  $g$  value very much greater than 2.0, indicating to rhombic distortions of the crystal field around Fe<sup>3+</sup> ions<sup>44</sup>. Some investigators<sup>45, 46</sup> suggested that these large  $g$  value of catalysts containing Fe<sup>3+</sup> ions is related to the coordination number, and the  $g\approx 4.2$  resonance signal is due to low symmetry (rhombic) sites of either tetrahedral or octahedral coordination<sup>44</sup>. Interestingly, with increase of Ce/Fe molar ratio, both of the two signals contributed to Fe<sup>3+</sup> almost disappear, corresponding to the the isolated free Fe<sup>3+</sup> gradually disappears<sup>37</sup>. In order to further elucidate the different iron species with Ce/Fe molar ratio, the evolution of this resonance line with the decrease of Fe/Ce molar ratio is following in the dependence of the EPR parameters. These parameters are: the peak-to-peak line width  $\Delta B$  and the line intensity approximated by  $I = I_0 (\Delta B)^2$  where  $I$  denotes the line height<sup>47</sup>. The corresponding variations of the separameters for the studied Cu/C<sub>1</sub>F<sub>x</sub> samples are presented in Fig. 3 for the resonance lines at  $g \approx 4.3$  (Fig. 3b) and  $g \approx 2.23$  (Fig. 3c), respectively. According to Fig. 3b, the line intensity of the resonance centered at  $g \approx 4.3$  increases with the decreasing of Fe/Ce molar ratio, the signal intensity being proportional to the quantity of EPR active species involves in the resonance absorption. The increase of this resonance line intensity at the same time with the decreasing of Fe/Ce molar ratio is due to the destruction of the configuration from the iron ions vicinities, which assures their magnetic isolation. The intensity of  $g \approx 2.23$  absorption line decreases with the

decreasing of Fe/Ce molar ratio, which further confirms that the formation of polymeric  $\text{Fe}^{3+}$  clusters are less. The line width evolution of the  $g \approx 4.29$  and  $g \approx 2.23$  resonance lines (Fig. 3b and 3c) shows a monotonically decrease with the decreasing of Fe/Ce molar ratio, which is associated to the dipole-dipole interactions and the interactions between iron ions and iron ions. Which manifest that with of Fe/Ce molar ratio decreasing, the content of distorted tetrahedrally coordinated isolated  $\text{Fe}^{3+}$  ions increases whereas that of the distorted octahedral coordinated polymeric  $\text{Fe}^{3+}$  clusters decreases. As the result, it is reasonable to conclude that isolated  $\text{Fe}^{3+}$  ions change into polymeric  $\text{Fe}^{3+}$  clusters with the increase of Fe/Ce molar ratio<sup>35</sup>. To sum up: the results of XRD, Raman and  $\text{H}_2$ -TPR in this work show, the copper, iron and ceria of  $\text{Cu/C}_1\text{F}_x$  existing in the form of  $\text{CuO}$ ,  $\text{Fe}_2\text{O}_3$  and  $\text{CeO}_2$ , respectively, corresponding to the integrity of the  $\text{Fe}_2\text{O}_3$  and  $\text{CeO}_2$  crystal structure. However, the EPR results shows only few copper ions could incorporate into the iron or ceria lattice in  $\text{Cu/C}_1\text{F}_x$  catalysts, due to the limitation of oxygen vacancies in the Ce-Fe support. On the other hand, the appropriate Ce/Fe molar ratio can create more oxygen vacancies, due to the formation of local nonequilibrium solid solution  $\text{CuO/C}_1\text{F}_x$  and therefore, more  $\text{Fe}^{3+}$  and  $\text{Ce}^{4+}$  could be substituted by  $\text{Cu}^{2+}$  ions.



**Fig. 3** EPR spectra of the studied copper catalysts on Fe-doped ceria supports (a). Composition dependence of line intensity and line width for  $g \approx 4.3$  (b) and  $g \approx 2.0-2.3$  (c)

**Fig. 4** depicted the  $\text{H}_2$ -TPR profiles for catalysts. The TPR profiles consist of three regions of  $\text{H}_2$  consumption, spanning the ranges 100–270, 270–500, and 500–900°C, associated with a reduction of  $\text{CuO}_x$ ,  $\text{Fe}_2\text{O}_3$ ,  $\text{FeO}$  and/or  $\text{CeO}_2$ , respectively<sup>23, 43, 48</sup>.  $\text{Cu/Ce}$  catalyst shows reduction peaks of  $\text{CuO}$  at 205, 241 and 296 °C, respectively, which indicated  $\text{CuO}$  fine dispersed in the  $\text{CeO}_2$  surface<sup>49</sup>. While Fe was introduced into  $\text{Cu/Ce}_1\text{F}_x$  catalysts, the TPR profiles for  $\text{Cu/Ce}$  became more complex. In the case of  $\text{Cu/Ce}_1\text{Fe}_{0.05}$  catalyst, there are two peaks of  $\text{CuO}$  at 160 and 192 °C,

## ARTICLE

## Journal Name

respectively, and a new peak appear at 523°C. Firstly,  $\text{Fe}_2\text{O}_3$  converts to  $\text{Fe}_3\text{O}_4$  at 300 - 450 °C and  $\text{Fe}_3\text{O}_4$  converts to FeO or Fe at 450 - 900°C, secondly, the temperature ranges of 450 - 600°C for Cu/Ce catalyst was not observed the reduction peaks of  $\text{CeO}_2$ . Hence, the peak at 523°C may be attributed to the reduction of the surface oxygen or lattice oxygen, which indicates that the strong interaction between Fe with Ce and the doping of Fe changed the oxygen structure of catalyst. While for Cu/ $\text{Ce}_1\text{Fe}_{0.5}$  catalyst, the reduction peaks of CuO at 162 and 195°C, a new peak appear at 322°C, attributed to the reduction of  $\text{Fe}_2\text{O}_3$  and the broad peak in the temperature range of 450-650°C attributed to the reduction of  $\text{Fe}_3\text{O}_4$  and lattice oxygen, respectively. The reduction peaks of CuO continue decrease to 144 and 177°C for Cu/ $\text{Ce}_1\text{Fe}_1$  catalyst, while the reduction peak of  $\text{Fe}_2\text{O}_3$  also reduced to 315°C, and the reduction peak of  $\text{Fe}_3\text{O}_4$  and lattice oxygen has shift to lower temperature. Notably, the reduction peaks of CuO and  $\text{Fe}_2\text{O}_3$  shift to higher temperature when continue increase the Fe/Ce molar ratio. For Cu/ $\text{Ce}_1\text{Fe}_5$  and Cu/ $\text{Ce}_1\text{Fe}_{10}$  catalysts, the reduction peaks of CuO increase to 183, 250°C and 191, 260°C, respectively. In the case of Cu/Fe catalyst, only a reduction peak for CuO at 215°C, and the TPR peak of  $\text{Fe}_2\text{O}_3$  at 320°C. Compared with Cu-Ce and Cu-Fe, the interaction of Fe and Ce exhibited complex reducibility of CuO. As reported in the literatures, these reduction peaks of CuO can be divided into different temperature range, which is related to the dispersed CuO species on the surface of catalyst<sup>34</sup>. The dispersed

oxygen, which is unstable structures and led to the copper species more easily reduced. Therefore, the dispersed copper species more easily incorporate into the cubic vacant sites of ceria when Ce/Fe molar is 1. Doping ceria with transition metals is a well-known way to modify the redox properties, enhance the oxygen mobility, and improve the catalytic activity<sup>23, 50, 51</sup>. Physical and catalytic properties of  $\text{Fe}_2\text{O}_3$ - $\text{CeO}_2$  binary systems can be modulated depending on the Fe/Ce molar ratio and preparation method. These observations may due to different interaction between copper and ceria-iron. From the above findings, it was suggested that ceria-iron mixed oxides with these molar ratios (1:1 and 1:0.5) readily promoted the reduction of copper species interacting with ceria-iron support. In summary, the difference in the reducibility of copper oxide should be related to the different coordinate environments of copper species, which is due to different surface structures of ceria and iron. Meanwhile, different Fe/Ce mole ratio changed the lattice oxygen of the catalyst structure.

### Effect of Fe/Ce molar ratio on the activity of catalysts

Fig. 5 showed the NO conversion and  $\text{N}_2$  selectivity with different Fe/Ce molar ratio as a function of temperature. For all the prepared catalysts, the NO reduction efficiency increased with temperature (Fig. 5a). The NO conversion of the catalyst supporter with only iron or ceria reached approximately 91% and 80% at 200 °C, respectively. The addition of ceria-iron mixed oxides significantly improved the reactivity compared with the Cu/Fe and Cu/Ce catalysts. In addition, the catalyst performance was depended on the Fe/Ce molar ratio in some extent. Overall, Cu/ $\text{C}_1\text{F}_1$  and gave the higher NO conversion than other catalysts. Especially at 200 °C, the difference in the activities was remarkable, following in this order: Cu/ $\text{C}_1\text{F}_1$  > Cu/ $\text{C}_1\text{F}_{0.5}$  > Cu/ $\text{C}_1\text{F}_5$  > Cu/ $\text{C}_1\text{F}_{0.1}$  > Cu/ $\text{C}_1\text{F}_{10}$  > Cu/Fe > Cu/Ce, which should be related to the difference of interaction between iron and ceria. In view of  $\text{N}_2$  selectivity over these catalysts (Fig. 5b), the remarkable difference could be observed below and above 100 °C. This might be resulted from the different active species at low and high temperatures. Additionally, the  $\text{N}_2$  selectivity followed in the order: Cu/ $\text{C}_1\text{F}_{0.1}$  > Cu/ $\text{C}_1\text{F}_{0.5}$  > Cu/Ce > Cu/ $\text{C}_1\text{F}_5$  > Cu/ $\text{C}_1\text{F}_1$  > Cu/ $\text{C}_1\text{F}_{10}$  > Cu/Fe. Obvious, the order of the  $\text{N}_2$  yield is not consistent with the NO conversion on Cu/ $\text{C}_1\text{F}_x$  catalysts at 200 °C. The reasons for these differences in the activity and  $\text{N}_2$  selectivity at low temperatures are that: above all, the addition amount of Fe should be the crucial factor,  $\text{N}_2$  selectivity are higher when the Fe/Ce molar

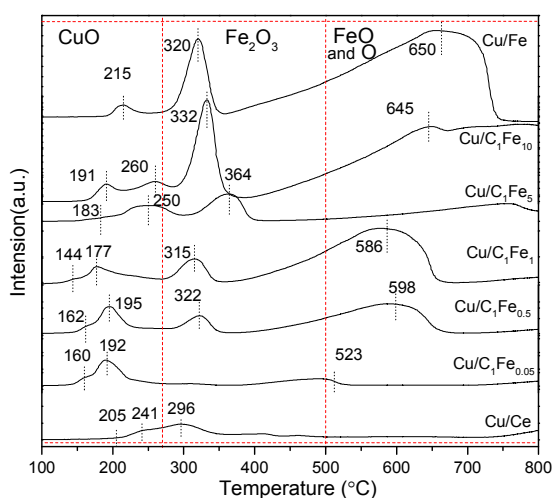
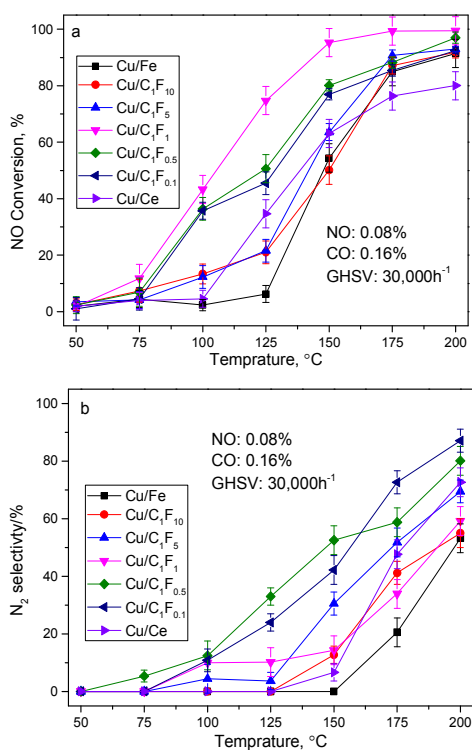


Fig. 4  $\text{H}_2$ -TPR profiles of the studied copper catalysts on Fe-doped ceria supports

copper species could incorporate into the cubic vacant sites of ceria and form a five-coordinated surface structure with the capping

ratio are less than or equal to 1 than the Fe/Ce molar ratio above 1, indicating a small amount of iron additive can more effectively convert NO to N<sub>2</sub>, the second, the specific surface area of the catalysts should be taken into consideration, corresponding to higher specific surface area helps to increase the effective Cu<sup>2+</sup> activity sites (Table 1). We compared the N<sub>2</sub> selectivity with the specific surface area of the Cu/C<sub>1</sub>F<sub>x</sub> catalysts, and found the N<sub>2</sub> selectivity followed the same order with the specific surface area, which indicated N<sub>2</sub> selectivity was sensitive to the structure of supports. Based on all the above results, Cu/C<sub>1</sub>F<sub>1</sub> catalyst displayed the better performance in activity correspondingly, which should be beneficial from the strong interaction among these components.



**Fig. 5** (a) NO conversion, (b) N<sub>2</sub> selectivity in CO + NO reaction over copper catalysts on Fe-doped ceria supports. (Conditions: GHSV = 30,000 h<sup>-1</sup>, 0.08% NO, 0.16% ppm CO)

In addition, compared with Cu/Fe, Cu/Ce sample has higher NO conversion efficiency and N<sub>2</sub> selectivity, which suggests that the NCO species may play an important role for NO reduction by CO. Notably, the N<sub>2</sub>O selectivity is also important with catalytic activity over Cu/C<sub>1</sub>F<sub>x</sub> catalysts. The amount of N<sub>2</sub>O over Cu/Fe was bigger and the temperature in the corresponding maximum amount of N<sub>2</sub>O was higher than in the case of Cu/Ce sample, which discloses the fact that Fe<sub>2</sub>O<sub>3</sub> phase is favored by N<sub>2</sub>O formation. Compared with

Cu/Fe and Cu/Ce catalysts, Cu catalysts on Fe-doped ceria show higher N<sub>2</sub> selectivity, especially Cu/C<sub>1</sub>F<sub>0.5</sub> and Cu/C<sub>1</sub>F<sub>0.1</sub>, indicating the modification of ceria by incorporation of lower Fe<sup>3+</sup> amount is beneficial for NO reduction by CO.

### In situ DRIFTS results of NO and CO co-adsorption with Cu/C<sub>1</sub>F<sub>1</sub> catalyst

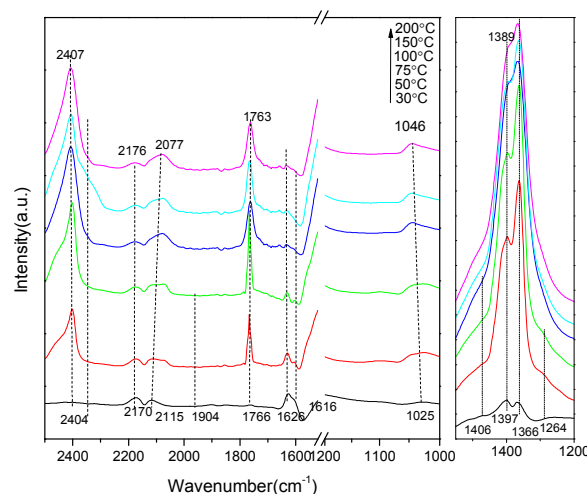


**Fig. 6** In situ DRIFTS spectra of NO and CO co-adsorption with Cu/C<sub>1</sub>F<sub>1</sub> catalyst with the catalysts from 30 °C to 200 °C

**Fig. 6** shows in situ DRIFTS results of NO and CO co-adsorption with Cu/C<sub>1</sub>F<sub>1</sub> catalyst as the temperature increases from 30 to 200 °C. The bridging bidentate nitrates display a NO<sub>2</sub> symmetric vibration mode at 1025 cm<sup>-1</sup>. Some bands observed at 1264 and 1366 cm<sup>-1</sup> can be assigned to the progressive accumulation of bidentate nitrates. These bands observed at 1347 - 1420 cm<sup>-1</sup> and 1600 - 1610 cm<sup>-1</sup> can be attributed to the vibration of the free nitrate ion and bridge nitrates, respectively, the former indicated that free nitrates acted as a stable inert species during the interaction of NO + CO<sup>52</sup>. The surface carbonate species appear at 1554 and 1567 cm<sup>-1</sup>, their intensities get stronger when the temperature increased to 200 °C and to the progressive accumulation of bidentate nitrates and carbonates. The band observed at 1605 cm<sup>-1</sup> can be attributed to the N = O stretching mode. While the band at 1766 cm<sup>-1</sup> can be assigned to vibrational modes of Cu-(NO)<sub>2</sub>, indicating that Cu ions acted as the active site for transforming nitrate oxides, which could promote the key step for the NO + CO reaction, i.e., the dissociation of NO. The gaseous NO molecules display a weak band at 1904 cm<sup>-1</sup>. Concerning the spectral features in the region of 2000 - 2500 cm<sup>-1</sup>, these bands at

## ARTICLE

around 2114 and 2176  $\text{cm}^{-1}$  can be assigned to  $\text{Cu}^+ - \text{CO}$  and carbonyl associated with cerium ions, respectively<sup>8</sup>, which were formed at room temperature via adsorbed CO with  $\text{Cu}^{2+}$ , indicating that the reduced copper species worked at lower temperature. The regions of 2400 - 2411  $\text{cm}^{-1}$  assigned to the accumulation of carbonate. Interestingly, no  $\text{N}_2\text{O}$  species appeared at all temperature, the formation of  $\text{N}_2\text{O}$  was in accordance with activity test results that low  $\text{N}_2$  selectivity at low temperature and high at high temperature on  $\text{Cu}/\text{C}_1\text{F}_1$  catalyst. Sugi et al.<sup>53</sup> associated the dependence of  $\text{N}_2\text{O}$  formation on the temperature by the following way: at the beginning of the reduction process, established the adsorption equilibrium between NO and  $\text{N}_2\text{O}$  and  $\text{N}_2\text{O}$  is displaced by NO before it is converted to  $\text{N}_2$ ; As the temperature rises, a part of the  $\text{N}_2\text{O}$  formed on the catalyst will be reduced to  $\text{N}_2$  before the displacement by NO, which was evidenced by  $\text{N}_2$  selectivity and in situ DRIFTS and the reaction mechanism was associated with the formation of  $\text{N}_2\text{O}$  over  $\text{Cu}/\text{C}_1\text{F}_1$  catalysts.

### In situ DRIFTS results of NO and CO adsorption with Cu/CF catalysts

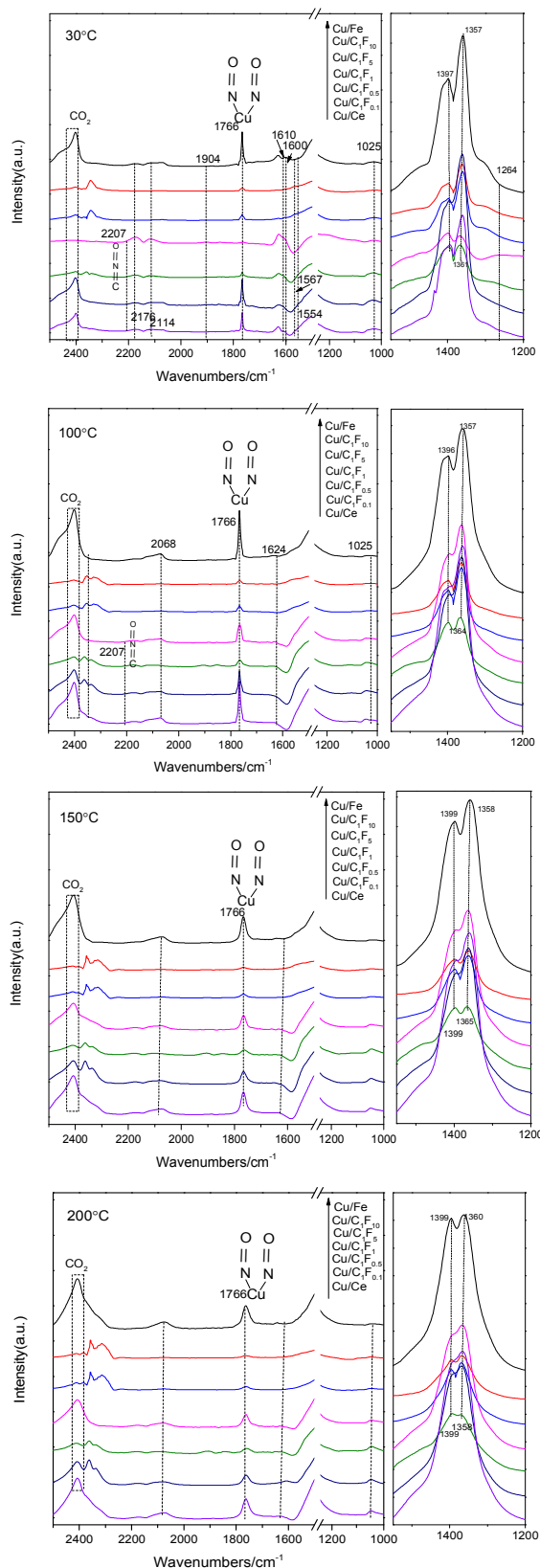


**Fig. 7** In situ DRIFTS spectra of NO and CO co-adsorption with  $\text{Cu}/\text{C}_1\text{F}_x$  catalyst with the catalysts from 25 °C to 200 °C

In order to clear the role of Fe addition for NO reduction by CO over these catalysts, in situ DRIFTS of NO and CO co-adsorption for these catalysts are collected at different Fe/Ce molar ratio with different temperatures, and the corresponding results are displayed in Fig.7. For Cu/Ce sample at 30 °C (Fig.7a), except for similar bands of Cu/C<sub>1</sub>F<sub>1</sub> sample. a new bands observed at 2207 cm<sup>-1</sup> can be assigned to the generation of intermediate isocyanates (NCO) species<sup>54</sup>, which indicated that copper plays an important role in the generation of oxygen vacancies on the basis of the generation mechanism of NCO in a significantly lower temperature range, which involving the dissociation of NO, followed by the reaction between the N atoms lying on the surface with the CO molecules and generate NCO species. However, with the introduction of Fe and the increase of Fe/Ce molar ratio, the NCO species disappear gradually, especially Cu/Fe sample. The reason is that the role of copper for NO dissociation is well known and the catalysts of rich-ceria have a higher effect in promotes NO desorption as N<sub>2</sub> at much lower temperatures than ceria-free catalysts<sup>55</sup>. In addition, free nitrate ion gradually shifted from 1395 and 1361 to 1397 and 1359 cm<sup>-1</sup> for Cu/Ce and Cu/Fe, indicated that the differences for NO adsorption on Cu<sup>2+</sup> and Fe<sup>3+</sup>, respectively. That bands assigned to the progressive accumulation of NO strengthen with the increase of Fe/Ce molar ratio, indicated the adsorption bond energy on Fe stronger than Ce, which suggested that the rich-iron phase had the greater ability to accelerate the NO desorption or/and rapid change in valence states of copper than rich-ceria during the reaction process.

Further increasing the temperature to 100, 150 and 200 °C (Fig.7b,7c and 7d), respectively, the adsorbed free nitrate ion specie (1396 cm<sup>-1</sup>) are steadily strengthen with the increase of the Fe/Ce molar ratio, indicated that iron adsorption sites possess stronger absorption ability of NO. The NCO species still exist in several catalysts, such as Cu/Ce, Cu/C<sub>1</sub>F<sub>0.1</sub>, Cu/C<sub>1</sub>F<sub>0.5</sub>. In addition, the decrease in peak intensity at 2207 cm<sup>-1</sup> may be due to decomposition of isocyanates at elevated temperatures<sup>13</sup>, suggesting NCO species are unstable. Especially above 150 °C, the peak disappear completely. Which is inconsistent with the xiao's results<sup>13</sup>, obviously, the difference mainly derive from the lower activity of Cu than Pt. It is interesting that the NCO species were not observed in rich-iron catalysts and further revealed NO easier to attach to the Fe. Simultaneously, some small weak peaks nitric

oxide species, as an intermediate of NO reduction by CO, appeared at around 2230 cm<sup>-1</sup> at rich-ceria catalysts. Daturi et al<sup>14</sup> suggest that the adsorption equilibrium between NO and N<sub>2</sub>O is established at the beginning of the reduction process, then N<sub>2</sub>O is displaced by NO before it is converted to N<sub>2</sub>; as the temperature is raised, a part of the N<sub>2</sub>O formed on the catalyst will be reduced to N<sub>2</sub> before the displacement by NO, which indicated the adsorption of NO is stronger than that of N<sub>2</sub>O. Additional, the addition of Fe obvious enhanced the intension of NO adsorbed, in other words, the addition of iron promoted the adsorption of NO and the reduction of copper oxide, the latter as the receptor of adsorbed CO. Cu<sup>2+</sup> ions also acted as NO adsorption sites, while Cu<sup>+</sup> ions acted as recipients of the O atoms produced through the dissociation of NO<sup>56</sup>. Therefore, rich-iron samples ensured an inhibition of the oxidation of CO by increased NO partial pressures because of the competitive adsorption of NO and CO<sup>54</sup>, which correspond to the NO reduction efficiency of Cu/Ce and Cu/Fe catalysts (Fig.3a).

### Possible reaction mechanism

In general, the dissociation of NO is the crucial step for NO removal by CO, and abundant oxygen vacancies can activate the N–O bond to promote this dissociation<sup>57</sup>. In our case, the different reducibility over Cu/CF catalysts possibly originated from their different surface structures, which corresponded to the copper species with different coordinated environments<sup>54</sup>. Combining with the above results and conclusion, the highly dispersed copper oxide was the active species in NO + CO reaction. When exposing the Cu/Ce catalyst to CO and NO mixture gases, the CO molecules preferred to adsorb on Ce<sup>4+</sup> sites rather than Cu<sup>2+</sup> sites, while the NO molecules preferred to adsorb on Cu<sup>2+</sup> sites rather than Ce<sup>4+</sup> sites. The scheme includes NO dissociation as two oxygen atoms from two NO molecules fill oxygen vacancies re-oxidizing the reduced ceria surface, while the nitrogen atoms recombine giving rise to a N<sub>2</sub> molecule<sup>14</sup>. The CO species adsorbed on Ce<sup>4+</sup> can combine with O radicals from the dissociation of NO on the adjacent oxygen vacancy to form CO<sub>2</sub>. With the formation of oxygen vacancies, Ce<sup>4+</sup> is restored to Ce<sup>3+</sup>, while Ce<sup>3+</sup> has better adsorption property of CO than Ce<sup>4+</sup>. Therefore, the NO conversion efficiency and CO oxidation rate increases, along with the temperature rises. The N<sub>2</sub>O was produced over Cu/Ce up to 100 °C.

Meanwhile, another scheme that isocyanates as the intermediates in the CO + NO reaction has been proposed based on the above analysis.

## ARTICLE

## Journal Name

First, the dissociation of NO on the oxygen vacancies of the copper sites, followed by the reaction between the N atoms lying on the surface with the CO molecules and generate NCO species. The unstable NCO species decompose quickly with the temperature goes up. However, the NCO species disappear completely when above 150 °C, which means the reaction process convert the scheme to the first scheme (N<sub>2</sub>O as the intermediate).

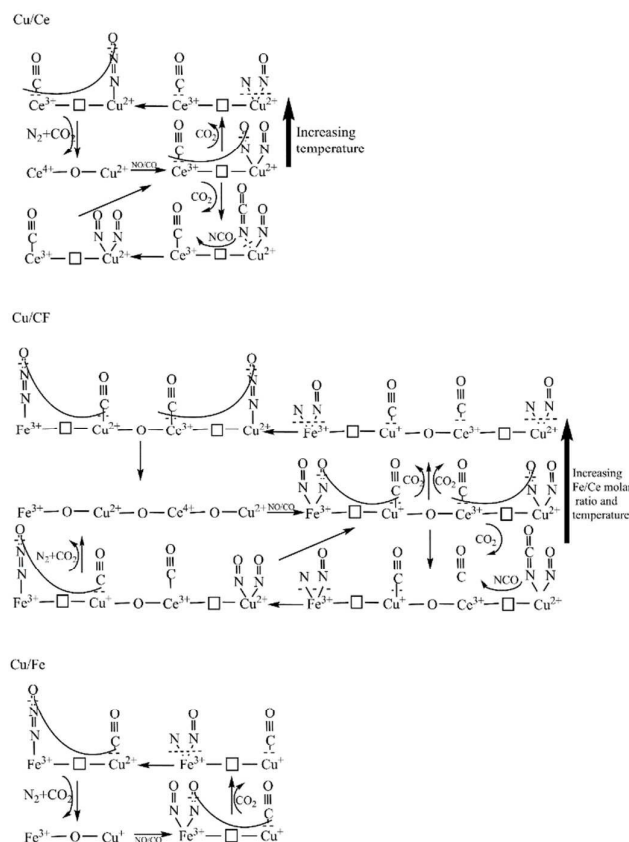


**Fig. 8** Possible reaction mechanisms of NO reduction by CO over copper catalysts on Fe-doped ceria supports with difference Ce/Fe molar ratio

When the Fe was introduced, the incorporation of lower Fe<sup>3+</sup> amount does not destroy the crystal structure of CeO<sub>2</sub>. Simultaneously, the addition of iron promoted the adsorption of NO and supplements inadequate the adsorption of NO based on a small amount of Cu activity sites, and then afford the O atoms produced through the dissociation of NO, and then, simultaneous, the rest of the N atoms combined with the adsorption of NO and to form N<sub>2</sub>O, eventually raising the reaction process. Thus, the addition of iron promoted the NO reduction by CO. However, the crystal structure of rich-iron samples is dominated by the crystal structure of Fe<sub>2</sub>O<sub>3</sub>.

The superabundant iron ensured an inhibition of the adsorption of CO by increased NO partial pressures and the CO adsorption diminishes. Especially for Cu/Fe<sub>2</sub>O<sub>3</sub>, Fe<sup>3+</sup> acts as the adsorption sites of NO, while Cu<sup>2+</sup>/Cu<sup>+</sup> acts as the adsorption sites of CO, which inhibited the formation of the NCO species based on the vulnerable to reduced of Cu<sup>2+</sup>. Hence, the mechanism of NO reduction by CO may accord with the first scheme (N<sub>2</sub>O as the intermediate). This suggests that NO chemisorption is deeply influenced by the co-existence of Fe and Ce. The cooperative activation of NO chemisorbed onto Cu<sup>+</sup> and Fe<sup>3+</sup> would be a key step, although further study should be needed to clarify the detailed reaction. To further understand the remarkable enhancement of the catalytic performance results from Fe/Ce molar ratio, the possible reaction mechanism is illustrated in Fig. 8.

## Conclusions

The work explored the effects of Ce/Fe molar ratio on the physicochemical properties of Cu/CF catalysts. It was found that copper oxide dispersed on Ce-Fe supports exhibited the different reducibility. The difference of Fe/Ce molar ratio reflect on the support's structure. Meanwhile, the ceria modification by incorporation of lower Fe<sup>3+</sup> amount is beneficial especially for NO conversion and the selectivity to N<sub>2</sub> as compared with the pure ceria and iron-rich ones. These were resulted from the difference in the strong interaction among the copper, iron–ceria support.

Additionally, DRIFT and activity tests results suggested that a dissociation mechanism for the CO + NO reaction was proposed over Cu/CF. The NO<sup>+</sup> species was further dissociated to intermediate N<sub>2</sub>O is the dominant reaction step. Nevertheless, there exists another mechanism that the interaction of chemisorbed NO and gaseous CO further to form the NCO intermediate originating over Cu/C<sub>1</sub>F<sub>x</sub> (x=0, 0.1 and 0.5). The addition of Fe obvious enhanced the intension of NO adsorbed and rich-iron samples inhibit the the oxidation of CO by increased NO adsorbed.

## Conflicts of interest

There are no conflicts to declare.

## Acknowledgements

The authors thank the National Natural Science Foundation of China (NO. 51776113 and NO. 51776114), Natural Science Foundation of Shandong Province (NO. ZR2017MEE035), the Key R&D Program Funds of Shandong Province (NO. 2017GSF17122), and the Foundation of Shandong University for Young Scholar's Future Plan (NO. 2017WLJH29) for the financial support.

## Notes and references

- C. Ge, L. Liu, Z. Liu, X. Yao, Y. Cao, C. Tang, F. Gao and L. Dong, *Catal. Commun.*, 2014, **51**, 95-99.
- Q. Yu, X. Yao, H. Zhang, F. Gao and L. Dong, *Appl. Catal. A-Gen*, 2012, **423**, 42-51.
- L. Liu, Y. Chen, L. Dong, J. Zhu, H. Wan, B. Liu, B. Zhao, H. Zhu, K. Sun and L. Dong, *Appl. Catal., B*, 2009, **90**, 105-114.
- C. A. Roberts, D. Prieto-Centurion, Y. Nagai, Y. F. Nishimura, R. D. Desautels, J. van Lierop, P. T. Fanson and J. M. Notestein, *J. Phys. Chem. C*, 2015, **119**, 4224-4234.
- C. Sun, Y. Tang, F. Gao, J. Sun, K. Ma, C. Tang and L. Dong, *Phys. Chem. Chem. Phys.*, 2015, **17**, 15996-16006.
- H. Simon, A. Reff, B. Wells, J. Xing and N. Frank, *Environ. Sci. Tech.*, 2014, **49**, 186-195.
- X. Cheng, X. Zhang, M. Zhang, P. Sun, Z. Wang and C. Ma, *Chem. Eng. J.*, 2017, **307**, 24-40.
- X. Cheng, M. Zhang, P. Sun, L. Wang, Z. Wang and C. Ma, *Green. Chem.*, 2016.
- J. Wang, X. Wang, J. Zhu, J. Wang and M. Shen, *Environ. Sci. Tech.*, 2015, **49**, 7965-7973.
- D. Rainer, M. Koranne, S. Vesecky and D. Goodman, *The J. Phys. Chem. B*, 1997, **101**, 10769-10774.
- M. Li, X. Wu, Y. Cao, S. Liu, D. Weng and R. Ran, *J. Colloid. Interf. Sci.*, 2013, **408**, 157-163.
- H.-o. Zhu, J.-R. Kim and S.-K. Ihm, *Appl. Catal. B*, 2009, **86**, 87-92.
- P. Xiao, R. C. Davis, X. Ouyang, J. Li, A. Thomas, S. L. Scott and J. Zhu, *Catal. Commun.*, 2014, **50**, 69-72.
- L. Ilieva, G. Pantaleo, N. Velinov, T. Tabakova, P. Petrova, I. Ivanov, G. Avdeev, D. Paneva and A. M. Venezia, *Appl. Catal. B*, 2015, **174-175**, 176-184.
- M. Haneda and H. Hamada, *J. Catal.*, 2010, **273**, 39-49.
- Q. Shen, G. Lu, C. Du, Y. Guo, Y. Wang, Y. Guo and X. Gong, *Chem. Eng. J.*, 2013, **218**, 164-172.
- P. C. Caldas, J. M. R. Gallo, A. Lopez-Castillo, D. Zanchet and J. M. C. Bueno, *ACS. Catal.*, 2017, **7**, 2419-2424.
- R. Zhang, W. Y. Teoh, R. Amal, B. Chen and S. Kaliaguine, *J. Catal.*, 2010, **272**, 210-219.
- G. Zafiris and R. Gorte, *J. Catal.*, 1993, **139**, 561-567.
- X. Wu, F. Lin, D. Weng and J. Li, *Catal. Commun.*, 2008, **9**, 2428-2432.
- M. Mrad, D. Hammoud, C. Gennequin, A. Aboukaïs and E. Abi-Aad, *Appl. Catal. A: Gen*, 2014, **471**, 84-90.
- X. Yao, Y. Xiong, W. Zou, L. Zhang, S. Wu, X. Dong, F. Gao, Y. Deng, C. Tang and Z. Chen, *Appl. Catal. B*, 2014, **144**, 152-165.
- Z. Liu, Z. Wu, X. Peng, A. Binder, S. Chai and S. Dai, *J. Phys. Chem. C*, 2014, **118**, 27870-27877.
- X. Li, X. Li, J. Li and J. Hao, *J. Hazard. Mater.*, 2016, **318**, 615-622.
- H. Zhang, A. Zhu, X. Wang, Y. Wang and C. Shi, *Catal. Commun.*, 2007, **8**, 612-618.
- J. Chen, J. Zhu, C. Chen, Y. Zhan, Y. Cao, X. Lin and Q. Zheng, *Catal. Lett.*, 2009, **130**, 254-260.
- Z. Yang, Y. Wei, Z. Fu, Z. Lu and K. Hermansson, *Surf. Sci.*, 2008, **602**, 1199-1206.
- E. V. Frolova, M. Ivanovskaya, V. Sadykov, G. Alikina, A. Lukashovich and S. Neophytides, *Prog. Solid. State Ch*, 2005, **33**, 317-325.
- Q. Yu, X. Wu, X. Yao, B. Liu, F. Gao, J. Wang and L. Dong, *Catal. Commun.*, 2011, **12**, 1311-1317.
- H. Zhu, M. Shen, F. Gao, Y. Kong, L. Dong, Y. Chen, C. Jian and Z. Liu, *Catal Commun.*, 2004, **5**, 453-456.
- F. J. Pérez-Alonso, M. López Granados, M. Ojeda, P. Terreros, S. Rojas, T. Herranz, J. L. G. Fierro, M. Gracia and J. R. Gancedo, *Chem. Mater.*, 2005, **17**, 2329-2339.
- A. Trovarelli, *Comment. Inorg. Chem.*, 1999, **20**, 263-284.
- N. Miki, Y. Kunihiko and M. Yuichi, *B. Chem. Soc. Jpn*, 1981, **54**, 975-979.
- Q. Yu, L. Liu, L. Dong, D. Li, B. Liu, F. Gao, K. Sun, L. Dong and Y. Chen, *Appl. Catal. B*, 2010, **96**, 350-360.
- L. Dong, B. Zhang, C. Tang, B. Li, L. Zhou, F. Gong, B. Sun, F. Gao, L. Dong and Y. Chen, *Catal. Sci. Tech.*, 2014, **4**, 482-493.
- D. Li, Q. Yu, S. S. Li, H. Q. Wan, L. J. Liu, L. Qi, B. Liu, F. Gao, L. Dong and Y. Chen, *Chem-Eur. J.*, 2011, **17**, 5668-5679.

## ARTICLE

## Journal Name

- 37 W. Wang, Q. Zhu, Q. Dai and X. Wang, *Chem. Eng. J* 2017, **307**, 1037-1046.
- 38 K. N. Rao, P. Venkataswamy and B. M. Reddy, *Ind. Eng. Chem. Res*, 2011, **50**, 11960-11969.
- 39 L. Qi, Q. Yu, Y. Dai, C. Tang, L. Liu, H. Zhang, F. Gao, L. Dong and Y. Chen, *Appl. Catal. B*, 2012, **119**, 308-320.
- 40 M. Fernandez-Garcia, A. Martinez-Arias, J. Hanson and J. Rodriguez, *Chem. Rev*, 2004, **104**, 4063-4104.
- 41 K. C. K. Lai and I. M. C. Lo, *Environ. Sci. Technol*, 2008, **42**, 1238-1244.
- 42 X. Zhu, K. Li, Y. Wei, H. Wang and L. Sun, *Energy. Fuel*, 2014, **28**, 754-760.
- 43 L. Liu, Z. Yao, B. Liu and L. Dong, *Journal of Catalysis*, 2010, **275**, 45-60.
- 44 S. P. Singh, R. P. S. Chakradhar, J. L. Rao and B. Karmakar, *J. Alloy. Compd*, 2010, **493**, 256-262.
- 45 R. S. Muralidhara, C. R. Kesavulu, J. L. Rao, R. V. Anavekar and R. P. S. Chakradhar, *J. Phy. Chem. Solids*, 2010, **71**, 1651-1655.
- 46 R. A. Eichel, H. Meštrić, K. P. Dinse, A. Ozarowski, J. van Tol, L. C. Brunel, H. Kungl and M. J. Hoffmann, *Magn. Reson. Chem*, 2005, **43**.
- 47 R. Stefan, P. Pascuta, A. Popa, O. Raita, E. Indrea and E. Culea, *J. Phys. Chem. Solids*, 2012, **73**, 221-226.
- 48 Z. Qu, L. Miao, H. Wang and Q. Fu, *Chem. Commun*, 2015, **51**, 956-958.
- 49 G. Avgouropoulos and T. Ioannides, *Appl. Catal. A-Gen*, 2003, **244**, 155-167.
- 50 A. Martínez-Arias, D. Gamarra, M. Fernández-García, A. Hornés and C. Belver, *Top. Catal*, 2009, **52**, 1425-1432.
- 51 Z. Liu, R. Zhou and X. Zheng, *J. Mol. Catal. A-Chem*, 2007, **267**, 137-142.
- 52 L. Wang, X. Cheng, Z. Wang, C. Ma and Y. Qin, *Appl. Catal. B*, 2017, **201**, 636-651.
- 53 Y. Sugi, N. Todo and T. Sato, *B. Chem. Soc. Jpn*, 1975, **48**, 337-338.
- 54 Y. Xiong, X. Yao, C. Tang, L. Zhang, Y. Cao, Y. Deng, F. Gao and L. Dong, *Catal. Sci. Tech*, 2014, **4**, 4416-4425.
- 55 Y. Xiaojiang, Y. XIONG, S. Jingfang, G. Fei, D. Yu, T. Changjin and D. Lin, *J. Rare. Earth*, 2014, **32**, 131-138.
- 56 V. I. Pârvulescu, P. Grange and B. Delmon, *Catal. Today*, 1998, **46**, 233-316.
- 57 T. Boningari, S. M. Pavani, P. R. Ettireddy, S. S. C. Chuang and P. G. Smirniotis, *Mol. Catal*, 2017.